CMS Physics Analysis Summary

Contact: cms-pag-conveners-susy@cern.ch 2015/10/15

Search for R-parity violating supersymmetry in dilepton channels

The CMS Collaboration

Abstract

Signatures of supersymmetry with R-parity violation (RPV) are searched for using proton-proton collisions at a centre-of-mass energy of 8 TeV. The analysis is based on the 2012 dataset taken with the CMS detector, corresponding to an integrated luminosity of 19.7 fb^{-1}. Final states consisting of two isolated leptons (electrons or muons) and jets are analyzed and interpreted in models of resonant slepton production via the RPV couplings λ'_{111} and λ'_{211}. The observation is in agreement with the expectation from standard model processes. Within modified versions of the cMSSM, including one of the two couplings as an additional non-zero parameter, exclusion limits on these couplings are set in the range of scalar masses m_0 up to 1.5 TeV and gaugino masses $m_{1/2}$ up to 2.5 TeV. Using simplified models, limits on the production cross section in the $m_{\tilde{\ell}}$-$m_{\tilde{\chi}^0_1}$ mass plane are determined.

1 Introduction

Supersymmetry (SUSY) [1–3] is an attractive extension of the standard model because of coupling unification, dynamic electroweak symmetry breaking and a solution to the hierarchy problem. In SUSY scenarios with R-parity violation, the lightest supersymmetric particle (LSP) is unstable and will decay into standard model particles. Due to the decay of the LSP, the signature of RPV SUSY differs strongly from standard SUSY searches since it exhibits no missing energy due to an escaping neutralino, and thus limits from searches for R-parity conserving SUSY typically do not apply. These scenarios may in addition allow for the resonant production of supersymmetric particles (e.g. sleptons) via RPV couplings.

This document describes a search for resonant production of first and second generation sleptons with the Compact Muon Solenoid (CMS) detector at the Large Hadron Collider (LHC). It is based on the $\sqrt{s} = 8\,\text{TeV}$ proton-proton collision dataset with an integrated luminosity of $19.7 \pm 0.5\,\text{fb}^{-1}$. The search focuses on final states consisting of two isolated leptons (electrons or muons) with the same charge and additional jets. Since the occurrence of this signature in standard model processes is very rare, it is well suited for the search for new physics.

This search extends the results from previous searches for second generation resonant production by the D0 [4] and CMS [5] collaborations and it is complementary to searches for RPV SUSY by the LEP (see references in [6]) and Tevatron experiments [7, 8].

2 CMS detector

The central feature of the CMS apparatus is a superconducting solenoid of 6 m internal diameter, providing a magnetic field of 3.8 T. A silicon pixel and strip tracker as well as a lead tungsten crystal electromagnetic calorimeter (ECAL) and a brass and scintillator hadron calorimeter (HCAL), each composed of a barrel and two endcap sections, are located within the superconducting solenoid volume. Muons are measured in gas-ionization detectors embedded in the steel flux-return yoke outside the solenoid. Extensive forward calorimetry complements the coverage provided by the barrel and endcap detectors.

The particle-flow event algorithm [9, 10] reconstructs and identifies each individual particle with an optimized combination of information from the various elements of the CMS detector. The energy of photons is directly obtained from the ECAL measurement, corrected for zero-suppression effects. The energy of electrons is determined from a combination of the electron momentum at the primary interaction vertex as determined by the tracker, the energy of the corresponding ECAL cluster, and the energy sum of all bremsstrahlung photons spatially compatible with originating from the electron track. The energy of muons is obtained from the curvature of the corresponding track. The energy of charged hadrons is determined from a combination of their momentum measured in the tracker and the matching ECAL and HCAL energy deposits, corrected for zero-suppression effects and for the response function of the calorimeters to hadronic showers. Finally, the energy of neutral hadrons is obtained from the corresponding corrected ECAL and HCAL energy.

Jets are clustered by the anti-k_T algorithm [11, 12] with a size parameter of 0.5. Their momentum is determined as the vectorial sum of all particle momenta in the jet, and is found from simulation to be within 5% to 10% of the true momentum over the whole p_T spectrum and detector acceptance. An offset correction is applied to jet energies to take into account the contribution from additional proton-proton interactions within the same bunch crossing. Jet energy corrections are derived from simulation, and are confirmed with in situ measurements of the

energy balance in dijet and photon+jet events. Additional selection criteria are applied to each event to remove spurious jet-like features originating from isolated noise patterns in certain HCAL regions. The jet energy resolution amounts typically to 15% at 10 GeV, 8% at 100 GeV, and 4% at 1 TeV, to be compared to about 40%, 12%, and 5% obtained when the calorimeters alone are used for jet clustering.

The electron momentum is estimated by combining the energy measurement in the ECAL with the momentum measurement in the tracker. The momentum resolution for electrons with $p_T \approx 45$ GeV from $Z \to e^+e^-$ decays ranges from 1.7% for nonshowering electrons in the barrel region to 4.5% for showering electrons in the endcaps [13].

Muons are measured in the pseudorapidity range $|\eta| < 2.4$, with detection planes made using three technologies: drift tubes, cathode strip chambers, and resistive plate chambers. Matching muons to tracks measured in the silicon tracker results in a relative transverse momentum resolution for muons with $20 < p_T < 100$ GeV of 1.3–2.0% in the barrel and better than 6% in the endcaps [14].

The missing transverse momentum vector is defined as the projection on the plane perpendicular to the beams of the negative vector sum of the momenta of all reconstructed particles in an event. Its magnitude is referred to as E_T^{miss}.

Performance details for the measurement of photons can be found in [15].

A more detailed description of the CMS detector, together with a definition of the coordinate system used and the relevant kinematic variables, can be found in Ref. [16].

3 Signal model

Constructing the most general minimal supersymmetric theory, one obtains lepton- and baryon-number violating terms in the superpotential [6]:

$$W_{LNV+BNV} = \underbrace{\frac{1}{2}\lambda_{ijk} L_i L_j \bar{E}_k}_{LLE\,\text{term}} + \underbrace{\lambda'_{ijk} L_i Q_j \bar{D}_k}_{LQD\,\text{term}} - \underbrace{\kappa^i L_i H_u}_{LH\,\text{term}} + \underbrace{\frac{1}{2}\lambda''_{ijk} \bar{U}_i \bar{D}_j \bar{D}_k}_{UDD\,\text{term}} \quad (1)$$

Here, the coefficients λ, λ' and κ allow lepton number violation (LNV), whereas the coefficient λ'' allows baryon number violation (BNV). These terms in conjunction lead to rapid proton decay, which has not been observed in nature [17]. In order to keep the proton stable, an additional symmetry is introduced. The most common choice for this symmetry is R-parity, which forbids all lepton- and baryon-number violating terms. However, theoretically equally well-motivated symmetries can replace R-parity in order to prevent proton decay [18, 19]. In these scenarios R-parity is not conserved, and thus such models are dubbed "R-parity violating (RPV) supersymmetry".

At the LHC, left-handed sleptons can be resonantly produced via the coupling coefficient λ'_{ijk} of the trilinear LQD term in the RPV superpotential, cf. eq. (1), where $i = 1, ..., 3$ denotes the lepton generation and $j, k = 1, ..., 3$ denotes the quark generation. Since protons are used in the initial state, the contribution for $j, k = 1$ is dominant. In this paper the search for first and second generation resonant slepton production via the λ'_{111} and λ'_{211} couplings is performed. Stringent bounds from leptonic pion decays exist for both couplings [6]. For the first generation coupling λ'_{111} additional bounds from neutrinoless double beta decay searches are more stringent for most of the parameter space. However, the LHC can improve these limits for certain parts

of the parameter space. Single coupling dominance for λ'_{111} or λ'_{211} [6] is assumed such that contributions from other RPV couplings can be neglected. For all considered values of λ'_{i11} in this analysis the slepton decay is effectively prompt.

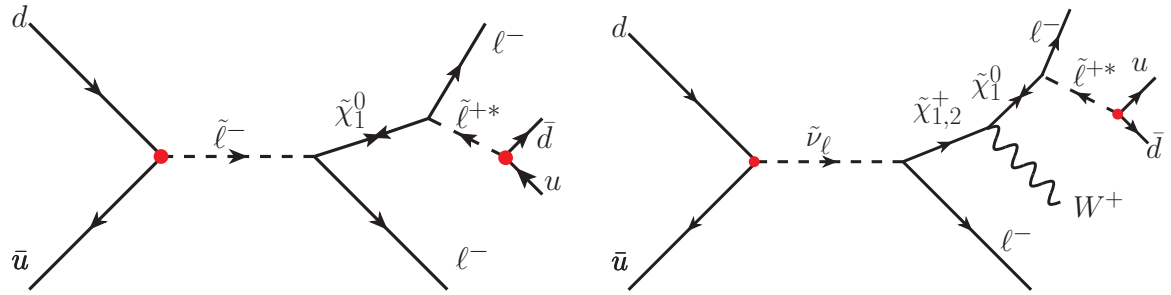

Figure 1: Resonant charged slepton (left) and neutral sneutrino (right) production and typical decay chain into final states with two same-sign and same-flavor leptons together with at least two jets. The R-parity violating vertices are marked by a red filled circle.

The search for resonant production of left-handed sleptons including charged sleptons as well as neutral sneutrinos concentrates on final states with two charged leptons and at least two jets. Fig. 1 illustrates the simplest possible Feynman diagrams leading to this final state, which is experimentally interesting because the presence of two leptons allows to discriminate the signal from background processes. One of the leptons is expected to be produced by the resonant slepton while the other lepton and two quarks resulting in jets are expected to be produced in the subsequent decay of the neutralino LSP. Due to the Majorana nature of the LSP, the two leptons have the same charge with about 50% probability, which allows to discriminate further against the background. There are multiple other diagrams involving heavier gauginos and longer decay chains which contribute to the desired final state with either additional leptons or jets. The different branching ratios depend on various signal properties, e.g. the involved particles' masses and the mixing of the gauginos. The charged sleptons and neutral sneutrinos of one generation are nearly mass-degenerated within the resolution of this search.

4 Signal simulation

The search results are interpreted in two different scenarios: a modified version of the cMSSM with one additional RPV coupling and a set of simplified models with the physical sparticle masses as free parameters.

For the first scenario, the particle mass spectrum and the couplings are calculated at the supersymmetry breaking scale using SOFTSUSY 3.3.5 [20, 21] under the premise of the modified cMSSM model with one additional RPV coupling (either λ'_{111} or λ'_{211}) while fixing the inputs at the unification scale. The simulated signal events have been generated with CALCHEP [22] in combination with PYTHIA 6 [23] using the CTEQ6.1L [24] parton distribution functions (PDF) and the Z2* [25] event tune. The detector response has been simulated with the GEANT4 [26] framework. The NLO corrections have been calculated according to Ref. [27]. The *k*-factors vary moderately over the entire considered parameter space from 1.27 to 1.39. Two mass scans are produced, one where the LQD coupling λ'_{111} is fixed to a value of 0.01 at the unification scale and one where λ'_{211} is fixed to that value instead. Since for small values of λ'_{i11} the production cross section scales with the square of the coupling, different λ'_{i11} values can be adopted after simulation for the limit setting. To cover a variety of *R*-parity violating constrained cMSSM scenarios, the m_0-$m_{1/2}$ parameter space is subdivided into a grid. The universal mass of scalar

particles m_0 is increased from 100 GeV to 1500 GeV and the universal mass of fermionic ones $m_{1/2}$ from 100 GeV to 2500 GeV. The size of each step is 100 GeV for both variables. All remaining parameters are constant throughout the entire grid and are chosen to be

$$A_0 = 0, \quad \tan\beta = 20, \quad \operatorname{sgn}\mu = +1.$$

The second scenario aims to avoid the restrictions of the cMSSM by using simplified models. Two of the dominating processes (see Fig. 2) to the dilepton and jets final state have been implemented in the event generator MADGRAPH [28]. For each of the two graphs and two channels additional mass scans were produced. Instead of using the full GEANT4 detector simulation these mass scans were produced using the CMS fast simulation package [29]. To match the reconstruction efficiencies of the full detector simulation additional scaling factors depending on the lepton kinematics are used.

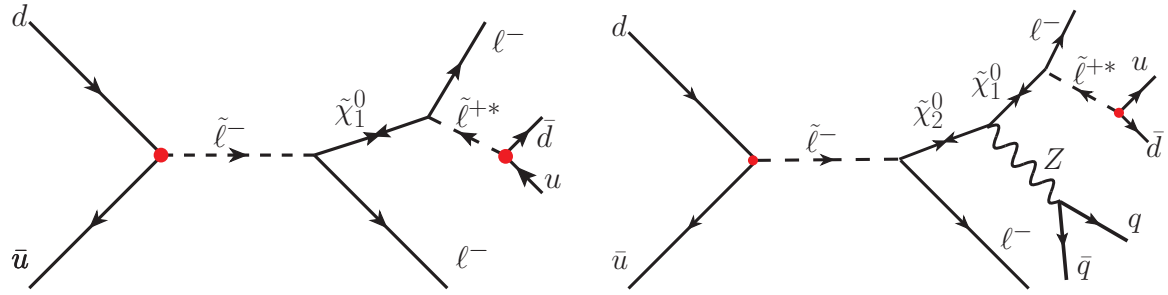

Figure 2: Resonant slepton $\tilde{\ell}$ production and decay via the simplest decay (left) and the decay via a heavier neutralino into a final state including 2 additional jets (right).

For the first graph the masses of the particles are scanned between:

- Mass of the resonantly produced slepton: 100-600 in 100 GeV steps and from there on up to 2.2 TeV in 200 GeV steps
- Mass of the lightest neutralino (always below the slepton mass): 50-150 GeV in 50 GeV steps for neutralino masses below 200 GeV and 200-1200 GeV in 100 GeV steps.

In the second graph the slepton decays into a heavier neutralino which subsequently decays into the lightest neutralino and an additional Z-boson. The lightest neutralino then decays in the same way as in the first graph. The mass scan is performed with the same masses as for the first diagram, while the mass of the heavier neutralino is given by:

$$m_{\tilde{\chi}_2^0} = m_{\tilde{\chi}_1^0} + x \times (m_{\tilde{\ell}} - m_{\tilde{\chi}_1^0}), \tag{2}$$

where the scaling parameter x is fixed to 0.25, 0.5 or 0.75. As an additional condition the mass gap between the two neutralinos has to be larger than the Z-mass.

5 Event selection

As a basic event selection, dielectron and dimuon triggers are used, where in both cases the leading lepton has a transverse momentum threshold of 17 GeV and the second lepton a transverse momentum threshold of 8 GeV. The p_T-threshold for leptons is optimized to retain high signal efficiency while keeping contributions from backgrounds small. To avoid turn-on effects,

the lepton p_T is required to be larger than the trigger thresholds. The resulting requirements are $p_T > 20\,\text{GeV}$ for the leading lepton and $p_T > 15\,\text{GeV}$ for the subleading lepton, where in average an efficiency of 98.1% is achieved for the dielectron and 94.7% for the dimuon trigger.

Events are required to have at least one well reconstructed vertex within $\Delta z < 24\,\text{cm}$ along the beam axis and radius $r < 2$ cm perpendicular to the beam axis around the nominal interaction point. If the event contains additional leptons (electrons or muons) above 10 GeV of transverse momentum or high noise in the electromagnetic and hadronic calorimeter cells it is discarded from the analysis.

Electrons are reconstructed in the pseudorapidity range up to $|\eta| < 2.5$ excluding the transition region between the barrel and endcap $1.44 < |\eta| < 1.57$. Muons have to be reconstructed both in the muon chambers and in the silicon tracker and reside in the pseudorapidity range of $|\eta| < 2.1$, avoiding endcap regions with high background contamination. Compared to the trigger requirements on the leptons, a stricter lepton identification is adopted in order to reduce contributions from misidentified leptons. An invariant mass of $M(\ell, \ell) > 15\,\text{GeV}$ is required to exclude events with J/ψ, Y, low-mass Drell-Yan processes as well as photon conversions. In the dielectron search a mass-window of 20 GeV around the Z-peak is also excluded to reduce the yield of events where one of the electrons is reconstructed with the wrong charge.

The charged leptons are required to be isolated. A particle flow based relative isolation criterion is used, where the sum of the energy deposits around the lepton in the tracker, electromagnetic and hadronic calorimeter are normalized to the lepton transverse momentum and corrected for additional activity of pileup. For electrons the isolation has to be smaller than 0.15 ($p_T > 20\,\text{GeV}$) or 0.1 ($p_T < 20\,\text{GeV}$), respectively. For muons its value is required to be less than 0.12.

The lepton with the highest (second highest) transverse momentum is denoted as e_1, μ_1 (e_2, μ_2).

Jets with a transverse momentum of $p_T > 30\,\text{GeV}$ in a range of $|\eta| < 2.4$ are selected. Further jet identification quality requirements [30] are applied and at least two jets in the event well separated from the leptons by $\Delta R > 0.4$ are required. Jets originating from b quarks are identified and vetoed using the combined secondary vertex (CSV) algorithm at the medium working point [31, 32]. Furthermore, muons are required to originate from the same vertex by requiring $\Delta z(\mu_1, \mu_2) < 0.8$ mm. Since little missing transverse energy (E_T^{miss}) is expected within the detector resolution, backgrounds such as $\mathrm{t\bar{t}}$ production with neutrinos in the final state can be partially suppressed by requiring $E_T^{\text{miss}} < 50\,\text{GeV}$, where the E_T^{miss} is obtained by means of particle flow objects.

After applying these selection requirements, the dominant background is expected to come from Drell-Yan production, followed by $\mathrm{t\bar{t}}$ production. At this stage and before applying any charge requirement the Drell-Yan simulation is scaled to match the event yield in the Z-peak region in the invariant $m(\ell_1, \ell_2)$ mass distribution. The left plots of Fig. 3 and 4 show the invariant mass distribution of the two leptons and the two leading jets after the scaling of the Drell-Yan simulation has been applied, representing the mass of the slepton resonantly produced in the primary interaction. A good agreement between data and simulation is observed.

The dominant Drell-Yan background is drastically reduced by requiring two same-sign leptons. After this requirement, $\mathrm{t\bar{t}}$ production with one of the two same-sign leptons either misidentified or originating from a semi-leptonic b-decay constitutes a major background component which can be further reduced by rejecting events with identified b-jets. For the dielectron case the main contributions come from QCD multi-jet and $\mathrm{W} + \text{jet}$ events where one or multiple jets are misidentified as electrons as well as from events where the charge of one of the electrons is mismeasured leading to a same-sign final state. Contributions from faked leptons have been

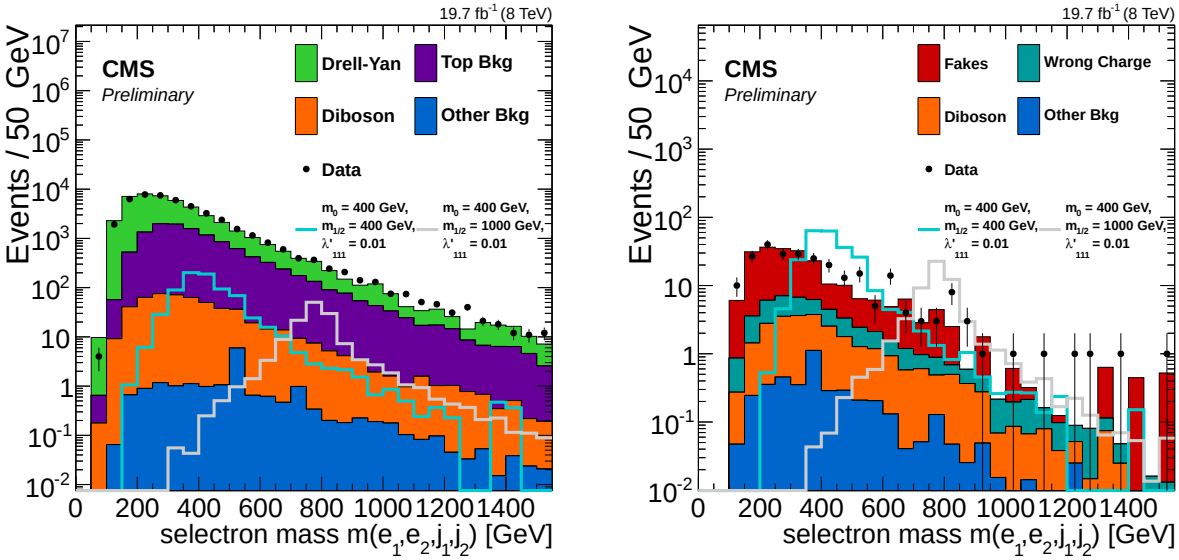

Figure 3: Invariant mass of the two electrons and jets before (left) and after (right) applying the b-tag veto and same-sign electron requirement. Data are compared to the expectation from simulation (left and right) and measured backgrounds (right). Signal distributions are shown for two different kinematic configurations.

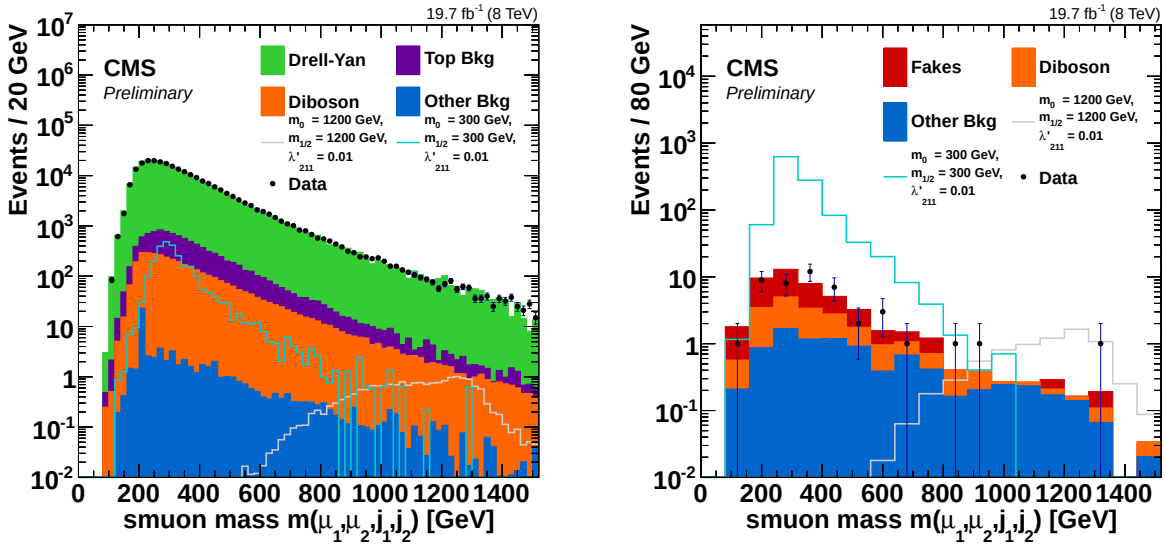

Figure 4: Invariant mass of the two muons and jets before (left) and after (right) applying the b-tag veto and same-sign muon requirement. Data are compared to the expectation from simulation (left and right) and measured backgrounds (right). Signal distributions are shown for two different kinematic configurations.

estimated with a data-driven method described below, and predictions for rare processes with prompt leptons are taken from simulation. For the dimuon search the dominant backgrounds consist of semi-leptonic $t\bar{t}$ events, where one of the leptons is misidentified and $WZ \to 3\ell + \nu$ events, where one of the leptons is either not reconstructed within the acceptance or fails the third lepton veto requirements. The resulting invariant mass distribution is shown in the right plot of Fig. 3 and Fig. 4.

The signal selection efficiency has been determined from simulation. Both the resonant production of a slepton as well as a sneutrino can lead to a same-sign two-lepton final state. Because of the large standard model production of dilepton final states, the analysis uses an $E_{\mathrm{T}}^{\mathrm{miss}}$ veto and focuses on the same-sign final state. Thus, decay chains containing neutrinos instead of charged leptons or decay chains resulting in opposite sign final states are neglected in order to enhance the signal to background ratio. The efficiency is thus of the order of a few percent for most of the considered parameter space. For low values of $m_{1/2}$, the neutralino is very light, boosted, and its decay products do not match the isolation criteria. This leads to small signal efficiencies. Since the lepton originating from the slepton decay is not sufficiently energetic, this search lacks sensitivity when the neutralino or chargino mass is close to that of the slepton. Because efficiencies are small for parts of the parameter space, they have been computed together with their uncertainties making use of the Wilson score interval [33].

5.1 Background estimates

After the full event selection, a small amount of background events from standard model processes remains. This background consists of three different components:

- "Non-prompt backgrounds" (Fakes)
  This background describes events with leptons from heavy-flavour decays, misidentified hadrons or electrons from non-matched photon conversions. Since these type of backgrounds are hard to model in simulation, a data-based method called "tight-to-loose" method is used to estimate their contribution to the search region. It is based on measuring the ratio of 'tight' to 'loose' leptons in a QCD enriched region. While tight leptons fulfill all selection steps as the leptons in the analysis, the loose leptons satisfy relaxed isolation and impact parameter criteria. Backgrounds which do not contain two prompt same-sign leptons are estimated by data events where one or both leptons used in the analysis only satisfy looser isolation and impact parameter criteria, but not the tight ones used in the analysis. These events are then weighted based on the "tight-to-loose" ratio depending on their transverse momentum and pseudo-rapidity. The remaining contributions from standard model processes which can produce same-sign events are subtracted using Monte Carlo (MC) simulations and the result of this subtraction provides an estimate of the non-prompt backgrounds. The main contributing processes are $W + \text{jets}$, $t\bar{t}$ and QCD multi-jet production. The method is validated by closure tests in simulation and leads to good agreement with data when applied to control regions.
- Standard model backgrounds with same-sign leptons
  There are very few standard model backgrounds which can lead to two prompt same-sign leptons and have altogether a very small cross section. Double-boson, triple-boson, $t\bar{t} + V$ and Higgs ($t\bar{t}H$, VH) production are considered as such and they constitute an irreducible background. Rare processes such as double parton interactions or two interactions in one bunch crossing can also lead to the same final state. All these processes are estimated from MC simulation. The main contributions arises from WZ production, for which agreement of the simulation with data

was cross-checked in a control region.

- Charge misidentification
  This background describes events with two prompt opposite-sign leptons where the charge of one of the leptons is misidentified yielding contributions to the same-sign final state. This only affects the electron channel since the charge misidentification for muons is negligible. As verified in data from $Z \to e^+e^-$ events the charge misidentification is well described in simulation and the wrong charge fraction obtained from the $t\bar{t}$ simulation is applied to opposite-sign data events to estimate the background yield from charge misidentified events.

Several MC samples are used for the background estimation (see above), the subtraction of non-fake contributions in the tight-to-loose ratio method and different cross-checks. The samples for the Drell-Yan, $W+$jets, top-pair with vector bosons ($t\bar{t}+V$), double boson (VV) and triple boson (VVV) production, where $V = W, Z$ stands for a W or a Z boson, are generated with MADGRAPH [28] interfaced to the event generator PYTHIA 6 [23] for parton shower, hadronisation and underlying event. Single and top quark pair production samples are generated with POWHEG [34–36]. The simulation of QCD multi-jet events and rare processes such as $t\bar{t}H$, ZH, WH, $W^{\pm}W^{\pm}$-production was done with PYTHIA 6. For the simulation of double parton scattering PYTHIA 8 was used. All samples include the simulation of pileup effects, were produced with the Z2* [25] event tune and the CTEQ6.1L [24] parton distribution functions and have been processed through a full simulation of the CMS detector based on GEANT4 [37].

6 Systematic uncertainties

Several sources of systematic uncertainties have been investigated. Their individual impact on the background prediction as well as the quadratic sum of all the uncertainties is summarized in Table 1.

Reconstructed object uncertainties of jet energy scale (JES) and resolution (JER) as well as lepton (electron and muon) energy scale and resolution are taken into account. Due to the fact that $E_{\mathrm{T}}^{\mathrm{miss}}$ is used in the event selection, all object energy variations have to be propagated into $E_{\mathrm{T}}^{\mathrm{miss}}$. The energy scales of leptons are shifted within their uncertainties and their resolution is smeared with a Gaussian function according to their uncertainties. The difference in event yield is taken as uncertainty.

Jet energy scale uncertainties have been evaluated following the procedure of [38]. The jet energy resolution in simulation is better than in data. The simulation has been corrected for this difference. Systematic uncertainties arise from matching ambiguities between jets of generated final state particles and reconstructed particle flow jets. The parameters of the b-tagging correction procedure are varied within the uncertainties found when computing the correction factors [31, 32].

Possible discrepancies in the lepton identification and isolation efficiencies between data and simulation are corrected by applying scale-factors to the simulated backgrounds, the uncertainty of these scale-factors is included as additional systematic uncertainty. The performance of the trigger might vary between the data and simulation. The trigger efficiency is determined using orthogonal jet trigger in data and simulation and a systematic uncertainty is assigned due to small differences between the two.

Further uncertainties on the background prediction from simulation are due to cross section uncertainties for the simulated backgrounds (50%), the luminosity measurement uncertainty

(see [39] for details), the choice of PDF and α_s used in the simulation and the pileup reweighting. Evaluation of PDF and α_s uncertainties have been performed following the PDF4LHC procedure [40] making use of the PDF sets CT10, MSTW2008 and NNPDF2.1. The systematic uncertainty on the pileup reweighting procedure for simulated events has been obtained by varying the number of interactions per event by $\pm 5\%$.

To obtain systematic uncertainties on the background estimate for fake leptons, the relative isolation criterion and the selection criteria for enriching the QCD multi-jet contribution while suppressing prompt leptons have been varied and for each variation the number of fake backgrounds has been re-evaluated. From the results of these variations and the closure tests a total systematic uncertainty of 50% on the fake estimate is assigned.

Table 1: Average impact of the systematic uncertainties on the event yield in the final search region. The first block of uncertainties is assigned to all simulated backgrounds. For the background prediction based on data the uncertainties given in the second block are taken. The quadratic sum of all individual sources (Σ) is shown in the third block.

source of sys. uncertainty	overall impact on final event yield [%]	
	electron channel	muon channel
luminosity	0.3	1.2
jet energy scale & resolution	0.2	1.7
b-tagging	0.1	0.3
lepton resolution & scale	0.3	0.1
identification & trigger efficiency	0.9	1.5
cross sections	5.6	23.1
PDF & pileup modeling	0.7	2.8
charge misidentification	6.1	-
data-driven background estimate	38.4	26.9
$\sum$	39.3	35.7

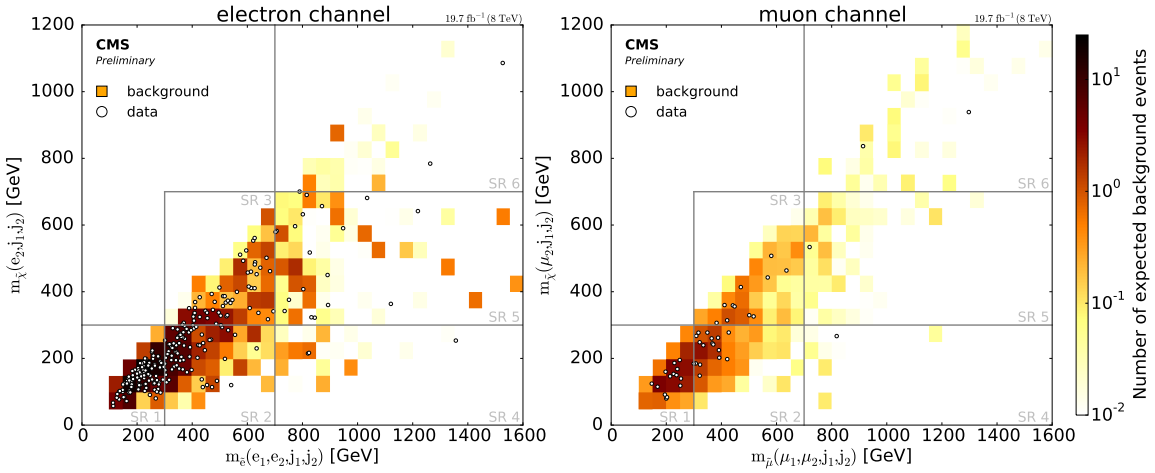

Figure 5: Background estimate and CMS data of the two-dimensional slepton and gaugino mass distribution for both electrons (left) and muons (right). All backgrounds are summed up and are shown as colored bins, while the data points are shown individually. The six bins are regarded as separate search regions SR 1-6 to improve the sensitivity for this analysis over the whole parameter space. The grey lines represent the borders of the individual search regions.

7 Results and interpretation

After the selection requirements we observe 255 candidate events in the dielectron final state (see Fig. 3-right). The data-driven estimate for the non-prompt electron background as well as Monte Carlo simulations for the remaining backgrounds yield a total background prediction of $N_{background} = 218.8 \pm 12.9$ (stat.) $\pm$ 84.7 (syst.) events. For the second generation search we observe 46 candidate events (see Fig. 4-right) which is in good agreement to the background prediction of $N_{background} = 47.0 \pm 1.8$ (stat.) $\pm$ 14.0 (syst.) events.

Further insight is gained by studying the distribution of events in the two-dimensional reconstructed slepton $m_{\tilde{\ell}}$ - reconstructed neutralino $m_{\tilde{\chi}}$ mass plane, where a peak is expected for the signal. To reconstruct the mass of the neutralino coming from the slepton decay, the lepton originating from this decay needs to be identified. Although there are in principle two choices, the lepton from the slepton decay is in most regions of the parameter space more energetic than the lepton from the LSP decay and can be identified as ℓ_1. Thus, the reconstructed slepton - neutralino mass plane is defined as $m_{\tilde{\ell}} = m(j_1, j_2, \ell_1^{\pm}, \ell_2^{\pm})$ $m_{\tilde{\chi}} = m(j_1, j_2, \ell_2^{\pm})$. The resolution of the reconstructed signal peak depends on the sparticle mass spectrum and the branching ratios to longer decay chains (e.g. Fig. 2-right). Its dependence on the lepton flavor is small, since the resolution of the different particle energies is dominated by the resolution of the jets. In general, the width of the reconstructed mass peak will be small for parameter points where the short decay chains dominate (e.g. around 5% for m_0 = 1000 GeV, $m_{1/2}$ = 2000 GeV ($m_{\tilde{\ell}} \approx 1600$ GeV)) and broader for parameter points where the longer decay chains are more frequent (e.g. around 16% for m_0 = 400 GeV, $m_{1/2}$ = 400 GeV ($m_{\tilde{\ell}} \approx 500$ GeV)).

The observed events in the data are compatible with the background expectation. No special structure can be observed. The parameter space is subdivided into six signal regions SR1 – SR6, corresponding to low, medium and high mass for the slepton and the neutralino, respectively. These regions, indicated in Fig. 5, are sensitive to different combinations of slepton and neutralino masses. The bin width is chosen such that the expected contribution from a signal can fit approximately into a single bin: The slepton and neutralino masses are reconstructed using the two highest jets. This works very well for short decay chains, but if longer decay chains are dominant the reconstructed masses will be lower than the generated ones due to the additional jets but most of the signal should be contained in the right signal region.

The corresponding event yields and their uncertainties for the six regions are given in Tables 2 and 3 for the dielectron and dimuon channel, respectively.

In SR3 and SR5 of the dielectron channel a small difference between the background expectation and data is observed. However, the difference is smaller than 2 σ in each region and the largest source of uncertainty is fully correlated between the two bins. Thus, this discrepancy is assumed to be a statistical fluctuation. Since the number of events from standard model backgrounds and data agree, there is no evidence for a signal. This result is interpreted by providing a set of exclusion limits. First an upper limit on the resonant slepton production cross section as a function of m_0 and $m_{1/2}$ is set (see Fig. 6-7), which is then translated into limits on the coupling parameters at the unification scale, λ'_{111} for resonant production of first generation sleptons and λ'_{211} for resonant production of second generation sleptons (see Fig. 8). For the second generation search, the results and the covered parameter space from previous analyses performed by D0 [4] and CMS [5] are shown for comparison (note that the D0 scan used different values for $\tan(\beta)$ and μ). In Fig. 9 the limit on the couplings is shown as a function of the physical masses of the slepton $m_{\tilde{\ell}}$ and the lightest neutralino $m_{\tilde{\chi}_1^0}$, for some example points in the parameter space the important masses and results are shown in Tab. 4. The LHC-style [41] CL_s method [42] is used to derive limits. As a test statistic, a profile Likelihood [43]

Table 2: First generation slepton: Summary of the six regions as displayed in Fig. 5. They are numbered starting on the left and progressing upwards from the lowest bin. Statistical and systematic uncertainties are added in quadrature. Correlations between the different sources of uncertainties are taken into account.

process group	SR 1		SR 2		SR 3	
fake estimate	89.22	$\pm$ 45.68	49.92	$\pm$ 26.08	19.77	$\pm$ 10.88
wrong charge	9.56	$\pm$ 2.29	8.29	$\pm$ 1.96	4.14	$\pm$ 0.95
VV	6.62	$\pm$ 3.40	8.18	$\pm$ 4.20	3.36	$\pm$ 1.73
rare	1.03	$\pm$ 0.55	1.10	$\pm$ 0.59	0.87	$\pm$ 0.48
$t\bar{t}+V$	0.16	$\pm$ 0.10	1.15	$\pm$ 0.74	0.52	$\pm$ 0.29
VVV	0.20	$\pm$ 0.11	0.35	$\pm$ 0.18	0.15	$\pm$ 0.08
$\sum$	106.79	$\pm$ 45.87	68.98	$\pm$ 26.51	28.81	$\pm$ 11.08
data	106		74		51	
process group	SR 4		SR 5		SR 6	
fake estimate	1.56	$\pm$ 1.52	6.74	$\pm$ 4.33	0.72	$\pm$ 1.01
wrong charge	0.24	$\pm$ 0.17	1.49	$\pm$ 0.57	0.47	$\pm$ 0.18
VV	0.16	$\pm$ 0.09	1.12	$\pm$ 0.58	0.30	$\pm$ 0.17
rare	0.06	$\pm$ 0.06	0.63	$\pm$ 0.36	0.30	$\pm$ 0.19
$t\bar{t}+V$	< 0.02		0.17	$\pm$ 0.11	0.01	$\pm$ 0.01
VVV	0.03	$\pm$ 0.02	0.09	$\pm$ 0.05	0.03	$\pm$ 0.02
$\sum$	2.05	$\pm$ 1.53	10.24	$\pm$ 4.42	1.83	$\pm$ 1.06
data	3		18		3	

Table 3: Second generation slepton: Summary of the six regions as displayed in Fig. 5. They are numbered starting on the left and progressing upwards from the lowest bin. Statistical and systematic uncertainties are added in quadrature. Correlations between the different sources of uncertainties are taken into account.

process group	SR 1		SR 2		SR 3	
fake estimate	13.4	$\pm$ 6.8	7.5	$\pm$ 3.8	3.7	$\pm$ 1.9
VV	5.6	$\pm$ 2.2	3.9	$\pm$ 1.7	2.4	$\pm$ 1.1
rare	1.72	$\pm$ 0.48	1.67	$\pm$ 0.52	1.90	$\pm$ 0.70
$t\bar{t}+V$	0.32	$\pm$ 0.14	0.43	$\pm$ 0.18	0.181	$\pm$ 0.090
VVV	0.31	$\pm$ 0.13	0.33	$\pm$ 0.15	0.153	$\pm$ 0.072
Σ	21.3	$\pm$ 7.2	13.8	$\pm$ 4.3	8.3	$\pm$ 2.4
data	15		16		11	
process group	SR 4		SR 5		SR 6	
fake estimate	0.19	$\pm$ 0.16	0.34	$\pm$ 0.25	0.21	$\pm$ 0.17
VV	0.045	$\pm$ 0.020	0.73	$\pm$ 0.36	0.22	$\pm$ 0.10
rare	0.101	$\pm$ 0.051	0.72	$\pm$ 0.26	0.80	$\pm$ 0.35
$t\bar{t}+V$	< 0.001		0.031	$\pm$ 0.015	0.063	$\pm$ 0.032
VVV	< 0.01		0.087	$\pm$ 0.040	0.027	$\pm$ 0.014
Σ	0.33	$\pm$ 0.19	1.91	$\pm$ 0.56	1.31	$\pm$ 0.46
data	1		1		2	

for a multi-bin Poisson counting experiment is used. The systematic uncertainties are modeled with log-normal distributions. All limits are set at the 95% confidence level.

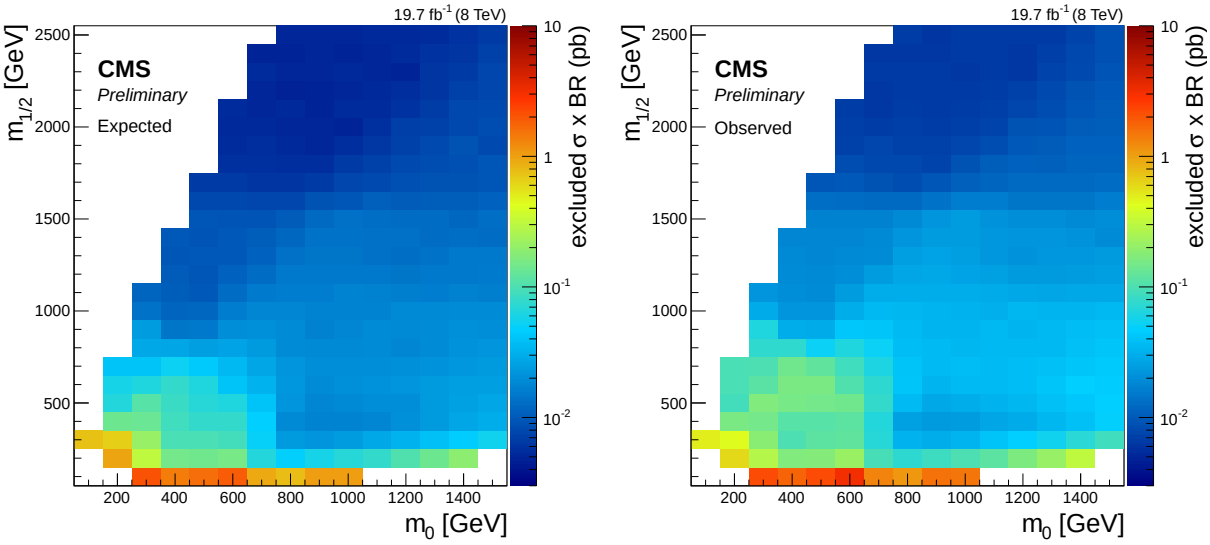

Figure 6: First generation slepton: Expected (left) and observed cross section limit (right) at 95% CL as a function of m_0 and $m_{1/2}$ for $A_0 = 0$, sign$(\mu) = +1$ and $\tan\beta = 20$.

Table 4: Sparticles masses and observed cross section and RPV coupling limits for both channels for a small subset of the covered parameter space. The limit on the RPV coupling is set at the unification scale.

m_0	$m_{1/2}$	$m_{\tilde{\ell}}$	$m_{\tilde{\chi}_1^0}$	cross section	cross section limit		coupling limit	
[GeV]	[GeV]	[GeV]	[GeV]	$\lambda'_{i11} = 0.01$ [fb]	electron [fb]	muon [fb]	λ'_{111}	λ'_{211}
200	200	245	76	$1.29 \cdot 10^4$	592	85.5	0.0021	0.0008
400	400	481	163	997	111	34.6	0.0033	0.0019
400	1000	772	427	121	22.0	4.20	0.0042	0.0018
1000	400	1031	165	39.1	24.5	13.5	0.0079	0.0059
1000	1000	1194	429	16.4	32.0	8.28	0.0140	0.0071
1500	1500	1787	656	1.51	19.6	11.9	0.0382	0.0290

In addition to the cMSSM scan, upper cross section limits based on a simplified model described in Section 4 are determined. In order to be less model dependent, the exclusion limits are set on the production cross section of the slepton times the branching ratio to particles shown in Fig.2-left, e.g. the lightest neutralino and a charged lepton for the first graph. The resulting observed cross section limits for the simplest graph can be seen in Fig. 10.

In the second graph the slepton decays into a heavier neutralino. This heavier neutralino decays into the lightest neutralino and an additional Z-boson. Even though these signal events typically result in more jets only the two jets with the highest p_T are used in the reconstruction of the sparticle masses. The spread in the reconstructed masses is wider for these events, but due to the large widths of the signal regions most of the signal is contained in a single region. The resulting observed cross section limits for a scaling parameter x=0.5 (see Eq. 2) can be seen in Fig. 11. The branching ratio used here is the branching ratio of the slepton decaying into a heavier neutralino and a charged lepton times the branching ratio of the heavier neutralino decaying into the lightest neutralino and a Z boson.

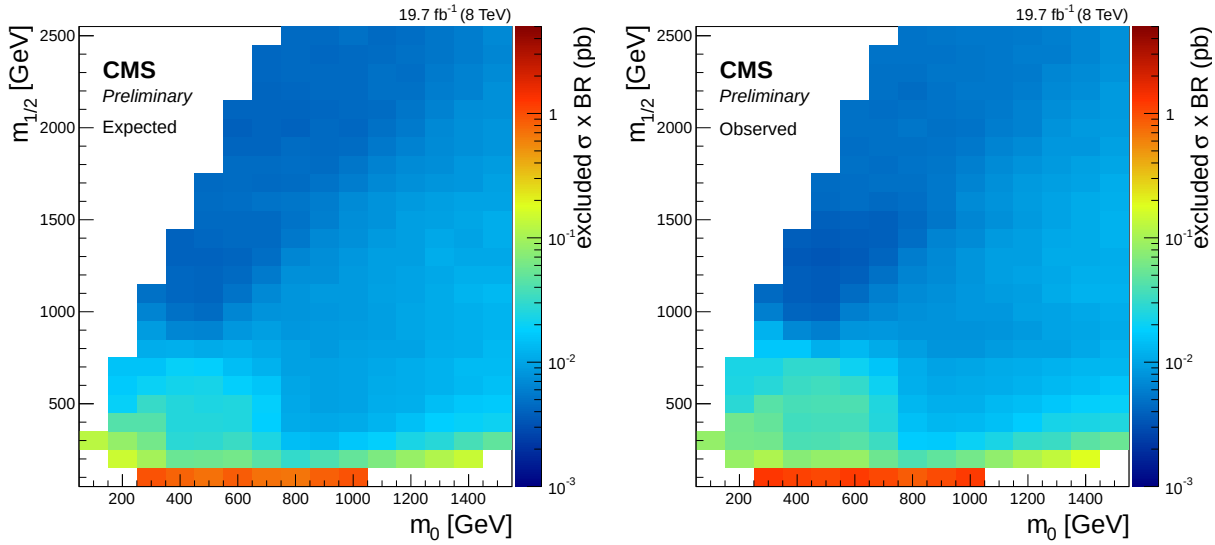

Figure 7: Second generation slepton: Expected cross section limit (left) and observed cross section limit (right) at 95% CL as a function of m_0 and $m_{1/2}$ for $A_0 = 0$, sign$(\mu) = +1$ and $\tan\beta = 20$.

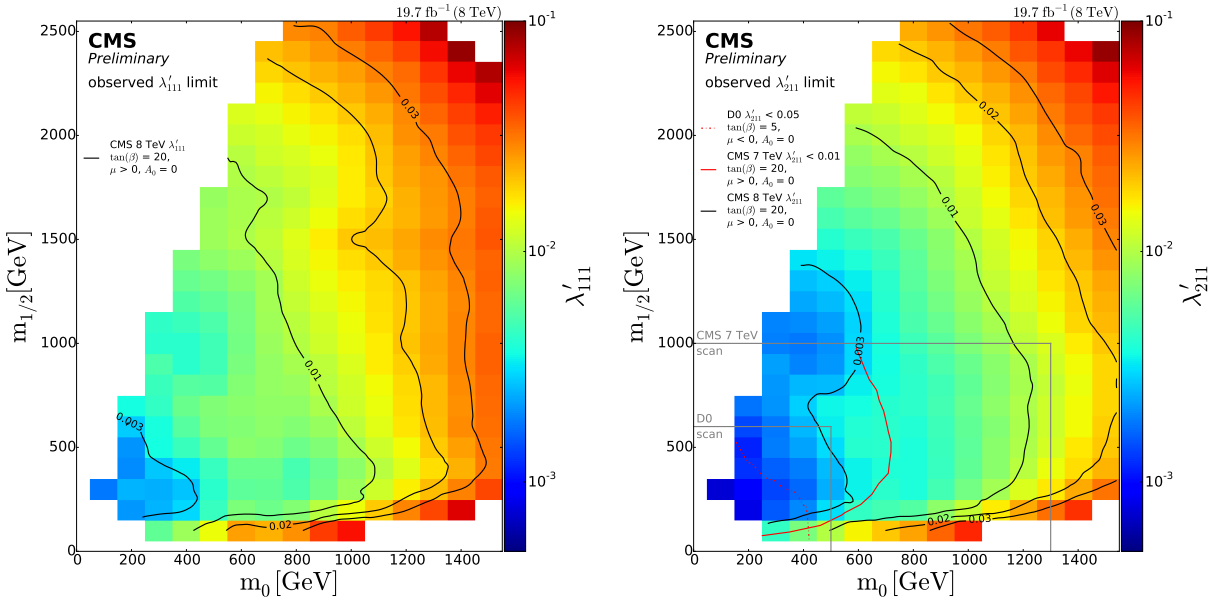

Figure 8: Translation of the observed cross section limit into an upper limit on the RPV couplings λ'_{111} (left) and λ'_{211} (right) at the unification scale. For comparison the covered parameter space and results from previous searches for resonant second generation slepton production performed by D0 [4] and CMS [5] are shown.

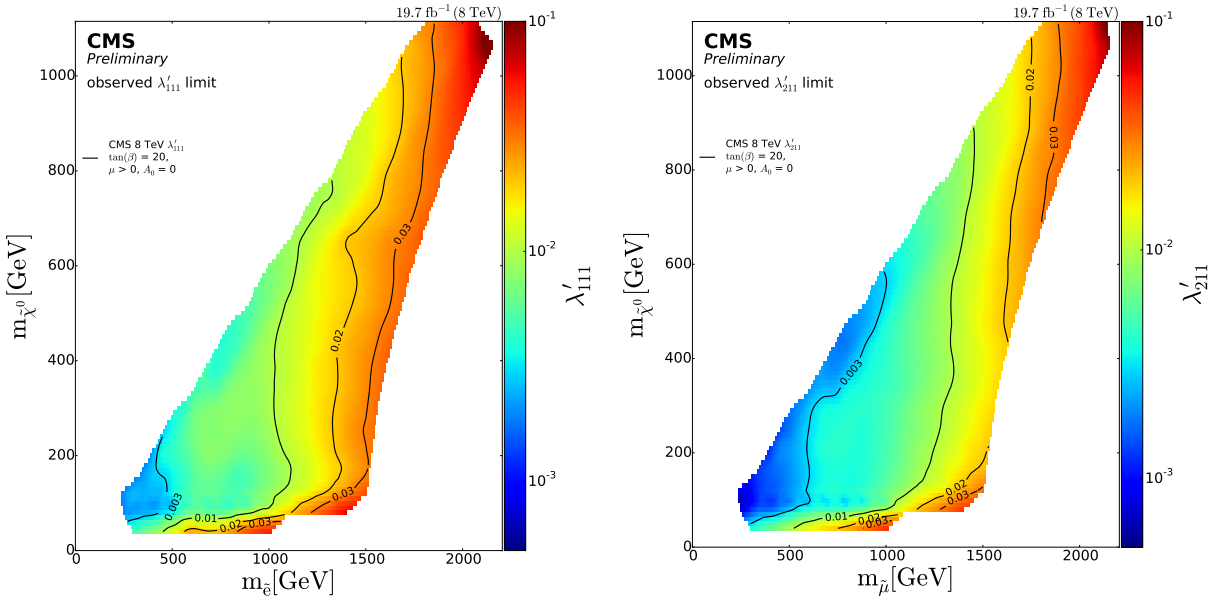

Figure 9: Upper limit on the RPV couplings λ'_{111} (left) and λ'_{211} (right) at the unification scale as a function of the physical masses in the two parameter scans.

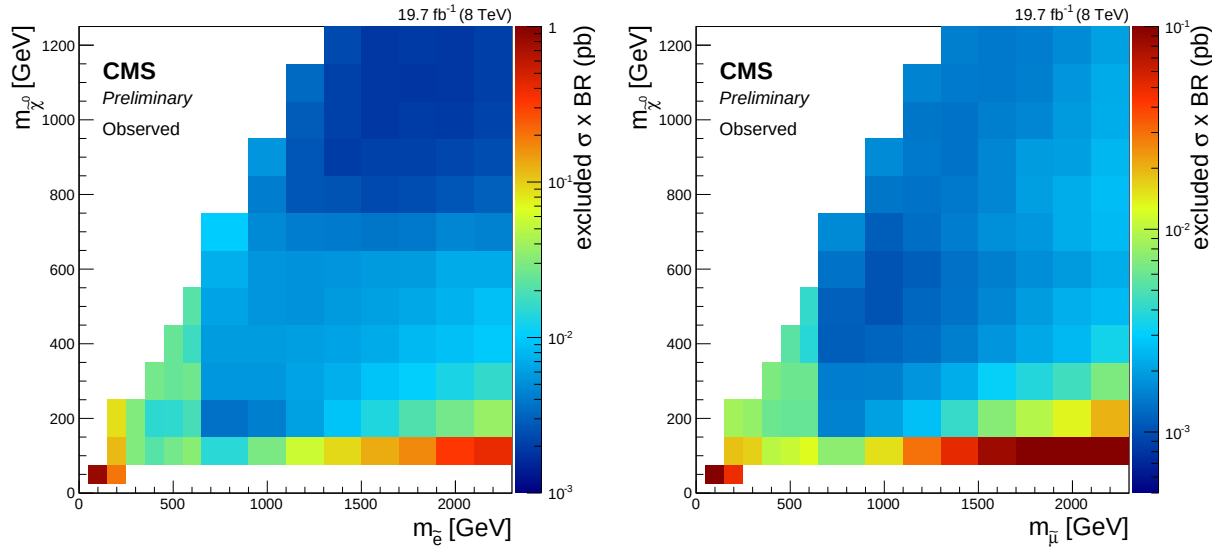

Figure 10: Observed cross section limits for the first simplified model for the dielectron (left) and the dimuon (right) channel. An upper limit is set on the production cross section times the branching ratio to the lightest neutralino and a charged lepton.

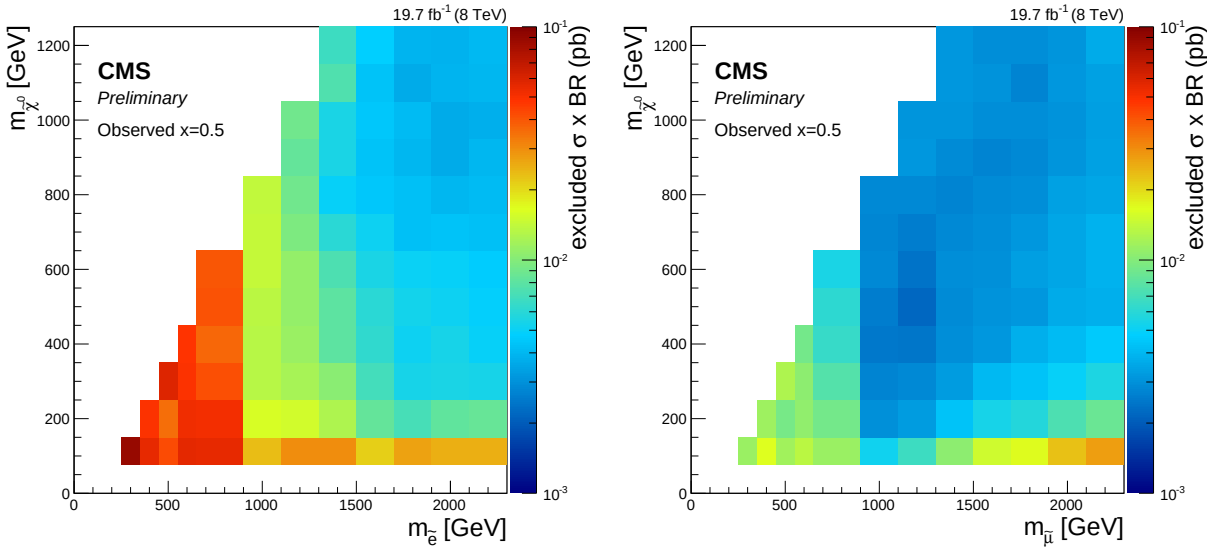

Figure 11: Observed cross section limit for the second simplified model graph. On the left the dielectron final state is used while the right one uses the dimuon final state. The limit is set on the production cross section times the branching ratio of the resonantly produced slepton decaying into a charged lepton, the lightest neutralino and an additional Z boson. The scaling parameter x is chosen to be 0.5.

8 Conclusions

A search for resonant production of sleptons ($\widetilde{\ell}$, $\tilde{\nu}_\ell$) via the R-parity violating couplings λ'_{111} and λ'_{211} with two same-sign leptons and at least two jets in the final state is presented. The kinematics of the signal is characterized by no missing transverse energy within the detector resolution. The search is based on the 2012 dataset with an integrated luminosity of 19.7 fb^{-1}, recorded with the CMS detector in proton proton collisions at a center of mass energy of $\sqrt{s} = 8$ TeV. The observed number of events agrees with the standard model prediction and exclusion limits are set within a modified version of the cMSSM with one additional R-parity violating coupling (λ'_{111} or λ'_{211}). Most stringent limits to date on these couplings in the range of scalar masses m_0 up to 1.5 TeV and gaugino masses $m_{1/2}$ up to 2.5 TeV are established. Compared to previous measurements from the D0 experiment [4] and the CMS experiment [5], the excluded parameter space for the resonant smuon production is extended considerably. Based on a simplified model approach, additional limits on the production cross section are set in the two-dimensional plane of neutralino $m_{\tilde{\chi}^0_1}$ and slepton mass $m_{\tilde{\ell}}$.

References

[1] H. P. Nilles, "Supersymmetry, Supergravity and Particle Physics", *Phys. Rept.* **110** (1984) 1, doi:10.1016/0370-1573(84)90008-5.

[2] H. E. Haber and G. L. Kane, "The Search for Supersymmetry: Probing Physics Beyond the Standard Model", *Phys. Rept.* **117** (1985) 75, doi:10.1016/0370-1573(85)90051-1.

[3] S. P. Martin, "A Supersymmetry primer", *Adv.Ser.Direct.High Energy Phys.* **21** (2010) 1–153, doi:10.1142/9789814307505_0001, arXiv:hep-ph/9709356.

[4] D0 Collaboration, "Search for resonant second generation slepton production at the Tevatron", *Phys.Rev.Lett.* **97** (2006) 111801, doi:10.1103/PhysRevLett.97.111801, arXiv:hep-ex/0605010.

[5] CMS Collaboration, "Search for RPV resonant slepton production", CMS Physics Analysis Summary CMS-PAS-SUS-13-005, 2013.

[6] R. Barbier et al., "R-parity violating supersymmetry", *Phys. Rept.* **420** (2005) 1–202, doi:10.1016/j.physrep.2005.08.006, arXiv:hep-ph/0406039.

[7] CDF Collaboration, "Search for R-parity violating supersymmetry using like-sign dielectrons in $p\bar{p}$ collisions at $\sqrt{s} = 1.8$ TeV", *Phys.Rev.Lett.* **83** (1999) 2133–2138, doi:10.1103/PhysRevLett.83.2133, arXiv:hep-ex/9908063.

[8] D0 Collaboration, "Search for R-parity violating supersymmetry via the LL anti-E couplings λ_{121}, λ_{122} or λ_{133} in $p\bar{p}$ collisions at $\sqrt{s}$ = 1.96-TeV", *Phys.Lett.* **B638** (2006) 441–449, doi:10.1016/j.physletb.2006.05.077, arXiv:hep-ex/0605005.

[9] CMS Collaboration, "Particle–Flow Event Reconstruction in CMS and Performance for Jets, Taus, and $E_{\mathrm{T}}^{\mathrm{miss}}$", CMS Physics Analysis Summary CMS-PAS-PFT-09-001, 2009.

[10] CMS Collaboration, "Commissioning of the Particle-flow Event Reconstruction with the first LHC collisions recorded in the CMS detector", CMS Physics Analysis Summary CMS-PAS-PFT-10-001, 2010.

[11] M. Cacciari, G. P. Salam, and G. Soyez, "The anti-k_t jet clustering algorithm", *JHEP* **04** (2008) 063, doi:10.1088/1126-6708/2008/04/063, arXiv:0802.1189.

[12] M. Cacciari, G. P. Salam, and G. Soyez, "FastJet User Manual", *Eur. Phys. J. C* **72** (2012) 1896, doi:10.1140/epjc/s10052-012-1896-2, arXiv:1111.6097.

[13] CMS Collaboration, "Performance of electron reconstruction and selection with the CMS detector in proton-proton collisions at $\sqrt{s} = 8$ TeV", *JINST* **10** (2015), no. 06, P06005, doi:10.1088/1748-0221/10/06/P06005, arXiv:1502.02701.

[14] CMS Collaboration Collaboration, "Performance of CMS muon reconstruction in pp collision events at $\sqrt{s} = 7$ TeV", *JINST* **7** (2012) P10002, doi:10.1088/1748-0221/7/10/P10002, arXiv:1206.4071.

[15] CMS Collaboration, "Performance of photon reconstruction and identification with the CMS detector in proton-proton collisions at $\sqrt{s} = 8$ TeV", (2015). arXiv:1502.02702. Submitted to *JINST*.

[16] CMS Collaboration, "The CMS experiment at the CERN LHC", *JINST* **3** (2008) S08004, doi:10.1088/1748-0221/3/08/S08004.

[17] Particle Data Group, K. A. Olive et al., "Review of particle physics", *Chin. Phys. C* **38** (2014) 090001, doi:10.1088/1674-1137/38/9/090001.

[18] L. E. Ibáñez and G. Ross, "Discrete gauge symmetries and the origin of baryon and lepton number conservation in supersymmetric versions of the standard model", *Nucl. Phys. B* **368** (1992) 3–37, doi:10.1016/0550-3213(92)90195-H.

[19] H. K. Dreiner, C. Luhn, and M. Thormeier, "What is the discrete gauge symmetry of the minimal supersymmetric standard model", *Phys. Rev. D* **73** (2006) 075007, doi:10.1103/PhysRevD.73.075007, arXiv:0512163.

[20] B. Allanach, "SOFTSUSY: a program for calculating supersymmetric spectra", *Comput. Phys. Commun.* **143** (2002) 305, doi:10.1016/S0010-4655(01)00460-X.

[21] B.C. Allanach and M.A. Bernhardt, "Including R-parity violation in the numerical computation of the spectrum of the minimal supersymmetric standard model: SOFTSUSY", *Comput. Phys. Commun.* **181** (2010) 232, doi:10.1016/j.cpc.2009.09.015.

[22] A. Belyaev, N. Christensen, A. Pukhov, "CalcHEP 3.4 for collider physics within and beyond the Standard Model", *Comput. Phys. Commun.* **184** (2013) 1729–1769, doi:10.1016/j.cpc.2013.01.014, arXiv:1207.6082.

[23] T. Sjostrand, S. Mrenna, and P. Z. Skands, "PYTHIA 6.4 Physics and Manual", *JHEP* **05** (2006) 026, doi:10.1088/1126-6708/2006/05/026, arXiv:0603175.

[24] J. Pumplin et al., "New generation of parton distributions with uncertainties from global QCD analysis", *JHEP* **0207** (2002) 012, doi:10.1088/1126-6708/2002/07/012, arXiv:hep-ph/0201195.

[25] R. Field, "Early LHC Underlying Event Data - Findings and Surprises", arXiv:1010.3558.

[26] S. Agostinelli and others, "Geant4 - A Simulation Toolkit", *Nucl. Instr. and Meth. A* **506** (2003) 250, doi:10.1016/S0168-9002(03)01368-8.

[27] H.K. Dreiner, S. Grab, M. Krämer, M. K. Trenkel, "Supersymmetric NLO QCD Corrections to Resonant Slepton Production and Signals at the Tevatron and the LHC", *Phys. Rev. D* **75:035003** (2007) doi:10.1103/PhysRevD.75.035003.

[28] F. Maltoni and T. Stelzer, "MadEvent: Automatic event generation with MadGraph", *JHEP* **0302** (2003) 027, doi:10.1088/1126-6708/2003/02/027, arXiv:hep-ph/0208156.

[29] S. Abdullin et al., "The fast simulation of the CMS detector at LHC", *J. Phys. Conf. Ser.* **331** (2011) 032049, doi:10.1088/1742-6596/331/3/032049.

[30] CMS Collaboration, "Jet Performance in pp Collisions at $\sqrt{s}$=7 TeV", CMS Physics Analysis Summary CMS-PAS-JME-10-003, 2010.

[31] CMS Collaboration, "Performance of b tagging at $\sqrt{s} = 8$ TeV in multijet, $\mathrm{t\bar{t}}$ and boosted topology events", CMS Physics Analysis Summary CMS-PAS-BTV-13-001, 2013.

[32] CMS Collaboration, "Identification of b-quark jets with the CMS experiment", *JINST* **8** (2013) P04013, doi:10.1088/1748-0221/8/04/P04013, arXiv:1211.4462.

[33] R. D. Cousins, K. E. Hymes, and J. Tucker, "Frequentist evaluation of intervals estimated for a binomial parameter and for the ratio of Poisson means", *Nuclear Instruments and Methods in Physics Research Section A: Accelerators, Spectrometers, Detectors and Associated Equipment* **612** (2010), no. 2, 388 – 398, doi:10.1016/j.nima.2009.10.156, arXiv:0905.3831.

[34] S. Alioli, P. Nason, C. Oleari et al., "NLO vector-boson production matched with shower in POWHEG", *JHEP* **07** (2008) 060, doi:doi:10.1088/1126-6708/2008/07/060, arXiv:0805.4802.

[35] P. Nason, "A new method for combining NLO QCD with shower Monte Carlo algorithms", *JHEP* **11** (2004) 040, doi:doi:10.1088/1126-6708/2004/11/040, arXiv:0409146.

[36] S. Frixione, P. Nason, and C. Oleari, "Matching NLO QCD computations with Parton Shower simulations: the POWHEG method", *JHEP* **11** (2007) 070, doi:doi:10.1088/1126-6708/2007/11/070, arXiv:0709.2092.

[37] GEANT4 Collaboration, "GEANT4: A Simulation toolkit", *Nucl.Instrum.Meth.* **A506** (2003) 250–303, doi:10.1016/S0168-9002(03)01368-8.

[38] CMS Collaboration, "Determination of Jet Energy Calibration and Transverse Momentum Resolution in CMS", *JINST* **6** (2011) doi:10.1088/1748-0221/6/11/P11002.

[39] CMS Collaboration, "CMS Luminosity Based on Pixel Cluster Counting - Summer 2013 Update", CMS Physics Analysis Summary CMS-PAS-LUM-13-001, 2013.

[40] PDF4LHC Group, "Recommendation for LHC cross section calculations", arXiv:1101.0538.

[41] ATLAS Collaboration and CMS Collaboration Collaboration, "Procedure for the LHC Higgs boson search combination in Summer 2011", Technical Report CMS-NOTE-2011-005. ATL-PHYS-PUB-2011-11, CERN, Geneva, Aug, 2011.

[42] T. Junk, "Confidence level computation for combining searches with small statistics", *Nucl.Instrum.Meth.* **A434** (1999) 435–443, doi:10.1016/S0168-9002(99)00498-2, arXiv:hep-ex/9902006.

[43] Particle Data Group Collaboration, "Review of particle physics", *Phys. Rev.* **D86** (2012) 010001, doi:10.1103/PhysRevD.86.010001.